Electron correlations—the origin of the CE phase in bilayer $La_{2-2x}Sr_{1+2x}Mn_2O_7$ manganites

2008 J. Phys.: Condens. Matter 20 365212

(http://iopscience.iop.org/0953-8984/20/36/365212)

J. Phys.: Condens. Matter **20** (2008) 365212 (11pp) doi:10.1088/0953-8984/20/36/365212

Electron correlations—the origin of the CE phase in bilayer $La_{2-2x}Sr_{1+2x}Mn_2O_7$ manganites

Krzysztof Rościszewski[1] **and Andrzej M Oleś**[1,2]

[1] Marian Smoluchowski Institute of Physics, Jagellonian University, Reymonta 4, PL-30059 Kraków, Poland
[2] Max-Planck-Institut für Festkörperforschung, Heisenbergstrasse 1, D-70569 Stuttgart, Germany

E-mail: roscis@if.uj.edu.pl and a.m.oles@fkf.mpg.de

Received 12 June 2008, in final form 27 July 2008
Published 14 August 2008
Online at stacks.iop.org/JPhysCM/20/365212

Abstract

We introduce the effective Hamiltonian which describes e_g electrons in doped bilayer $La_{2-2x}Sr_{1+2x}Mn_2O_7$ manganites and study magnetic and charge order using correlated wavefunctions. The Hamiltonian includes: the kinetic energy, the crystal field splitting between x^2-y^2 and $3z^2-r^2$ orbitals, on-site interactions—Coulomb U and Hund's exchange J_H between e_g electrons, antiferromagnetic superexchange interaction $J' > 0$ between t_{2g} core $S = 3/2$ spins, and finally the coupling between e_g electrons and Jahn–Teller local modes. The model reproduces reasonably well the evolution of magnetic order with increasing hole doping x in the experimentally accessible range from $x = 0.3$ up to $x = 0.9$. Electron correlations are found to be of crucial importance for the stability of the recently experimentally identified CE phase in a half-doped ($x = 0.5$) bilayer (with zig-zag ferromagnetic chains in each plane coupled antiferromagnetically with neighbouring chains in the same and in the other layer).

1. Introduction

The properties of doped colossal magnetoresistance manganites are puzzling and not completely understood in spite of much effort put forward both in theory and in experiment [1, 2]. They are characterized by a complex interplay of charge, spin, orbital and lattice degrees of freedom. The main difficulty in the theoretical description of this class of compounds is related to this simultaneous interplay of several degrees of freedom. The early attempts, considering only some of them, such as for instance the Jahn–Teller (JT) effect supplemented by Hund's exchange (but neglecting other on-site Coulomb interactions) [1, 3], or considering only on-site Coulomb interaction U (while neglecting Hund's exchange J_H), or including only the coupling to the lattice due to the JT effect [4], turned out to be insufficient to account for the complexity of experimental data. In fact, both large Coulomb interactions and the orbital interactions which emerge due to the JT distortions are responsible for the observed magnetic and orbital order in $LaMnO_3$ [5, 6]. In addition, it has also been realized that the core t_{2g} electrons, even if localized (passive), still play an essential role in the observed magnetic order and may tip the balance between different types of order due to the antiferromagnetic (AF) superexchange between them [7–10]. Therefore, one cannot select a subset of the interactions as being essential, with the others (of secondary importance) being added only to get quantitative corrections. The actual magnetic, orbital and charge order in this class of compounds is a result of subtle balance between all the numerous factors.

On the theoretical side, the multiband models and/or approaches based on *ab initio* local density approximation (LDA) computations extended by either static corrections due to local Coulomb interaction U (LDA + U) [7, 11–13], or by dynamical mean-field theory (LDA + DMFT method) [14], capture the essential features of the electronic structure and are a good starting point for a more sophisticated theoretical description of perovskite manganese oxides, making use of the many-body theory. In the past a well known difficulty with the latter approach, however, was the multitude of unknown (Hamiltonian) parameters which had to be estimated or computed independently (with a prohibitive cost). Therefore, recent progress, in electronic structure calculations on the one

hand and in experiment on the other, is of enormous help here as the relevant parameters can be deduced, and the model presented below is well supported. We emphasize that we do not intend to achieve one hundred percent fidelity, but we would like to identify the physical mechanisms responsible for the particular types of order observed in doped bilayer manganites using a well supported effective model (note that a description of a particular phase stable at a single value of doping would be possible with much simpler models which contain only a few parameters).

In the present paper we use such an effective model (featuring only Mn sites renormalized by the presence of surrounding oxygens) for the description of itinerant e_g electrons which is believed to include all the essential interactions present in doped manganites [9]. We do not develop new concepts but rather put together the interactions tested in numerous papers and investigate which ground state is stable for a particular doping level when local electron correlations and the JT effects are both included. Previously this model was used in context of monolayer manganites [10].

In this paper we analyze two-dimensional (2D) bilayer manganites such as $La_{2-2x}Sr_{1+2x}Mn_2O_7$. Indeed, while an isotropic ferromagnetic (FM) phase in doped perovskite systems [15] is described by the orbital liquid [16], this class of compounds provides one of the best examples of the complexity of manganite physics. Their experimental properties, in particular information about the type of magnetic order and phase diagram (versus doping), were described in detail in a series of papers [17–24]. We present the effective model which, in our opinion, is a necessary compromise between simplicity and the requirement to include all basic and relevant factors responsible for the physical properties of bilayer $La_{2-2x}Sr_{1+2x}Mn_2O_7$ compounds. We assume that the t_{2g} orbitals of Mn^{3+} ions are occupied by three 'core' electrons with total spin $S = 3/2$—the core electrons are treated here as classical and frozen. The only active electrons which contribute to charge dynamics and may induce charge order are the e_g ones. This approximation for $3/2$ core spins has been tested before and found to perform reasonably well [2, 8, 9].

The paper is organized as follows. First, we introduce (in section 2) a *realistic* model for e_g electrons in bilayer manganites which includes the electron Coulomb interactions and the local potentials acting on them due to JT distortions (section 2). In this section we also present the method to treat electron correlation effects in the ground state beyond the Hartree–Fock (HF) approximation. The numerical results are presented and analyzed in section 3. Here we address a question as to which values of the parameters of the effective Hamiltonian are appropriate to account for the experimentally observed situation. Finally, section 4 contains a short summary of the paper and gives general conclusions.

2. The effective model Hamiltonian

We study strongly correlated electrons in doped bilayer manganites $La_{2-2x}Sr_{1+2x}Mn_2O_7$ (with $0.3 < x < 0.88$), using an effective model describing only Mn sites, where the state of surrounding oxygens is simulated by an effective potential at each site. It is believed that a realistic effective Hamiltonian (which acts in the subspace of low energy e_g states) can be derived by a procedure of mapping the results of HF, or LDA + U, or all-electron *ab initio* calculations obtained within a more complete approach. A local basis at each manganese site is given in such a model by two Wannier orbitals of the e_g symmetry ($x^2 - y^2$ and $3z^2 - r^2$) [11].

We investigate the system by using a Hubbard-like Hamiltonian $\mathcal{H}$ for e_g electrons which experience local fields due to local JT distortions and due to their interactions with the core t_{2g} spins. The form of the Hamiltonian is the following:

$$\mathcal{H} = H_{\rm kin} + H_{\rm cr} + H_{\rm int} + H_{\rm spin} + H_{\rm JT}. \tag{1}$$

It consists of the kinetic energy $H_{\rm kin}$, the crystal field splitting of e_g orbitals $H_{\rm cr}$, on-site Coulomb interactions $H_{\rm int}$, spin interactions $H_{\rm spin}$, and the JT part $H_{\rm JT}$. The first three terms concern solely the e_g subsystem, while the other two may be seen as external fields acting on them. This model and/or the essential parts of it were studied earlier in numerous papers [1, 3, 9–11, 25–27].

The kinetic and one-body part, called for brevity the kinetic energy,

$$H_{\rm kin} = -\tfrac{1}{4}t_0 \sum_{\{ij\}\|ab,\sigma} \{3d^\dagger_{ix\sigma}d_{jx\sigma} + d^\dagger_{iz\sigma}d_{jz\sigma} \pm \sqrt{3}(d^\dagger_{ix\sigma}d_{jz\sigma} + d^\dagger_{iz\sigma}d_{jx\sigma})\} - t_0 \sum_{\{ij\}\|c,\sigma} d^\dagger_{iz\sigma}d_{jz\sigma}\,, \tag{2}$$

is expressed using the basis of two e_g orbitals

$$x^2 - y^2 \equiv |x\rangle, \qquad 3z^2 - r^2 \equiv |z\rangle, \tag{3}$$

per site—in short notation x and z orbitals—and includes anisotropic phase dependent hopping [28]. Here $d^\dagger_{i\mu\sigma}$ are creation operators for an electron in orbital $\mu = x, z$ with spin $\sigma = \uparrow, \downarrow$ at site i, and summations include the nearest neighbour pairs of indices $\{ij\}$. The effective Mn–Mn hopping matrix elements arise due to the hybridization with oxygen orbitals on Mn–O–Mn bonds, and are therefore anisotropic and orbital dependent [28]. The hopping occurs between nearest in-plane neighbours ($\{ij\} \parallel ab$) and nearest neighbours from the upper and lower plane of the bilayer ($\{ij\} \parallel c$). The $\pm$ is interpreted as plus sign for the bond $\{ij\}$ parallel to the crystal axis a and minus for $\{ij\}$ parallel to the crystal axis b. As mentioned above, the kinetic energy is supplemented by the crystal field term

$$H_{\rm cr} = \tfrac{1}{2}E_z \sum_{i\sigma} (n_{iz\sigma} - n_{ix\sigma}), \tag{4}$$

which describes anisotropy between two e_g states in the 2D bilayer geometry (here $n_{i\mu\sigma} = d^\dagger_{i\mu\sigma}d_{i\mu\sigma}$ are the corresponding electron number operators). In the present convention used in equation (4), for positive values of crystal field parameter ($E_z > 0$) the occupancy of $|x\rangle$ orbital is favoured over the occupancy of $|z\rangle$ orbital.

The interactions between e_g electrons are given by [29]

$$H_{\rm int} = U \sum_{i\mu} n_{i\mu\uparrow}n_{i\mu\downarrow} + \left(U - \tfrac{5}{2}J_{\rm H}\right) \sum_i n_{ix}n_{iz} - \tfrac{1}{2}J_{\rm H} \sum_i (n_{ix\uparrow} - n_{ix\downarrow})(n_{iz\uparrow} - n_{iz\downarrow}) - J_{\rm H} \sum_{i\mu} S^z_i (n_{i\mu\uparrow} - n_{i\mu\downarrow}). \tag{5}$$

We use the usual convention that the on-site Coulomb interaction element is denoted as U, and Hund's exchange interaction element is $J_{\rm H}$ [6]. The first three terms stand for the interaction between e_g electrons, while the last one describes Hund's exchange coupling between the e_g electrons and core t_{2g} spins. The Hund's exchange terms, as given above in equation (5), correspond, in fact, to a rather crude approximation. Namely, here for simplicity we use the Ising interaction: instead of the spin–spin scalar products, we take the product of two zth components of spin only. Thus, we explicitly break the spin rotational symmetry and fix the quantization axis along the zth spin component. This is not an approximation, however, when the mean-field (MF) treatment of the $SU(2)$ symmetric Heisenberg term is employed in order to determine the HF wavefunction. In fact, this form of Hund's interaction is consistent with the MF procedure, where the remaining transverse terms do not contribute, and also significantly simplifies the computation of the correlation energy as described below. However, the price one has to pay is that the phases with spatial variation of local spin quantization axis are completely excluded from the present considerations.

As mentioned above, the frozen t_{2g} core spins in equations (5) and (6) are replaced by discrete classical Ising variables $S_i^z = \pm 3/2$ [8, 9]. They interact through the effective AF superexchange interaction $J' > 0$ [3, 6, 9, 13, 28] which follows from the respective itinerant model for t_{2g} electrons in the strongly correlated regime [5], and we write the Ising term

$$H_{\rm spin} = J' \sum_{\langle ij \rangle} S_i^z S_j^z. \tag{6}$$

Here, unlike in equation (2), the sum over bonds $\langle ij \rangle$ includes each pair of nearest neighbour sites only once.

Finally, the JT part in equation (1) is

$$H_{\rm JT} = \sum_i \left\{ g \left(Q_{2i} \tau_i^x + Q_{3i} \tau_i^z \right) + \tfrac{1}{2} K \left(Q_{2i}^2 + Q_{3i}^2 \right) \right\}, \tag{7}$$

where the pseudospin operators τ_i^α ($\alpha = x, z$) at site i are defined by

$$\begin{aligned} \tau_i^x &= \sum_\sigma (d_{ix\sigma}^\dagger d_{iz\sigma} + d_{iz\sigma}^\dagger d_{ix\sigma}), \\ \tau_i^z &= \sum_\sigma (d_{ix\sigma}^\dagger d_{ix\sigma} - d_{iz\sigma}^\dagger d_{iz\sigma}), \end{aligned} \tag{8}$$

and $\{Q_{2i}, Q_{3i}\}$ denote the active JT deformation modes of the oxygens around a given Mn ion at site i—they lift the degeneracy of e_g orbitals (and modify the orbital splitting due to the crystal field E_z). For simplicity, the fully symmetric (breathing mode) deformation is neglected in $H_{\rm JT}$, as well as additional minor quadratic couplings (for a more elaborate form of $H_{\rm JT}$ including the next-neighbour couplings as applied to manganites see for example [30]).

The parameters we used for the numerical calculations are taken from the existing literature. Although their estimates by various authors differ from each other, we selected the commonly accepted values. Thus we take an effective $(dd\sigma)$ hopping element $t_0 = 0.4$ eV following refs. [5, 10], while other estimations in the literature fall in the range $0.2 < t_0 < 0.6$ eV [1, 4, 9, 31–33]. Reasonable values of the effective on-site Coulomb repulsion range from $U = 3.5$ eV, deduced by Kovaleva *et al* [34] from the analysis of the optical spectral weights, to about $U = 5.0$ eV, which is expected in the effective spin–orbital model [6]. The smallest value found in the literature is 1.7 eV [11] obtained for the effective model neglecting Hund's exchange interaction (this value corresponds in fact to $U - 3J_{\rm H}$). Park *et al* [12] estimated U to be about 3.5 eV using their photoemission data (for the undoped perovskite $LaMnO_3$), while a much smaller value ∼2.0 eV was deduced earlier by Okimoto *et al* [35] from the optical conductivity data (for lightly doped $La_{1-x}Sr_xMnO_3$). Other values suggested in the literature are close to 5.0 eV [9], or to 5.5 eV [5]. Thus we see that the data on U used in the literature are widely scattered. In fact, the screening of the atomic value of U is considerable and the realistic value of U in the manganites is difficult to estimate. We will argue that reasonable agreement between the predictions of our model and the experimental data requires an intermediate value in the range $U = (8 \pm 2)t_0$.

Coming to Hund's exchange coupling $J_{\rm H}$, we notice that it is widely believed that the ratio $J_{\rm H}/t_0$ is somewhat larger than unity [1]. This indeed follows from the realistic parameter estimates given by various authors, with $J_{\rm H}$ varying from the atomic value of 0.9 eV [32, 36] down to 0.7 eV [5] and 0.67 eV [6], and even being as small as $J_{\rm H} = 0.5$ eV (again following reference [34] and assuming a larger screening). Let us emphasize that the ratio of $J_{\rm H}/U$ plays a crucial role in the nature of superexchange interactions between e_g electrons [5, 6]. In our computations we used values ranging from 0.5 to 0.9 eV (also a value of zero was studied in order to emphasize the role of Hund's term). The realistic value applicable to $La_{2-2x}Sr_{1+2x}Mn_2O_7$ is (in our opinion) expected to be close to 0.7 eV.

For the JT interaction parameters in equation (7) we adopt $K = 13$ eV Å^{-2} and $g = 3.8$ eV Å^{-1}, following [4, 37–39]. For the parameter J' in equation (6) we adopted the value 4.0 meV. Smaller values do not seem to reproduce well the occurrence of FM phases for smaller dopings ($0.3 < x < 0.4$). The value $J' = 4.0$ meV correlates reasonably well with the value of 3.0 meV as obtained from the fit to spin waves in $LaSrMnO_4$ (in the framework of a slightly different model) in [40]. Other studies [19, 33, 41] (again partly in the framework of slightly different models) suggest a value between 3.0 and 4.0 meV. The actual ratio $J'/t_0 \approx 0.01$ in principle falls into the range 0.01–0.1 which was recommended by Dagotto, Hotta and Moreo in their review article [1]. Other papers suggest that J' should be smaller, namely ∼3.0 meV [6] or ∼1.0–1.5 meV [34], but even values as small as 0.9 meV [4] or 0.4 meV [12], have been suggested.

The last parameter we consider is the crystal field splitting E_z, for which we assumed the value $E_z = 0$ in most of our calculations (i.e., degenerate x and z orbitals). Again we justify this choice by verifying that this value seems to reproduce best the experimental data. However, other non-zero values were also suggested [12, 13, 42]. Thus we also studied (in numerous test computations) such values as $E_z = \pm 0.5t_0$ and $E_z = \pm 0.25t_0$, but in each case the final results invariably fall too far away from experiment.

We studied the ground states of $4 \times 4 \times 2$ clusters in bilayer geometry (containing $N = 32$ sites) with periodic boundary conditions along crystallographic a and b axes, and free boundary conditions along the crystallographic c axis, assuming different hole concentration $x = 1 - n$ (away from half-filling $n = 1$, where n is e_g electron density), changing from $x = 0.3$ up to $x = 0.88$—all these dopings are well covered by the experimental data [17–24]. (Larger clusters such as $8 \times 8 \times 2$ are feasible only for isolated computations but certainly not for computations involving the thousands of different initial conditions which were necessary in the present case in order to catch the multitude of closely spaced metastable ground states in a non-homogeneous system such as the bilayer manganite.) First, the calculations within the HF approximation employing a single-determinant wavefunction were performed to establish the ground state wavefunction $|\Psi_{\rm HF}\rangle$. Thereby numerous starting initial conditions were used (in order to get unbiased results we a used few hundred of them for each point in the parameter space).

In the next step each of the obtained HF wavefunctions $|\Phi_0\rangle$ was modified to improve the energy and to include the effects of local electron correlations. We used exponential local ansatz for the correlated ground state [43],

$$|\Psi\rangle = \exp\Big(\sum_m \eta_m O_m\Big)|\Phi_0\rangle, \tag{9}$$

where $\{\eta_m\}$ are variational parameters, and $\{O_m\}$ is a set of local correlation operators. The quality of the variational wavefunction $|\Psi\rangle$ depends on the choice of the correlation operators. The variational parameters η_m are found by minimizing the total energy

$$E_{\rm tot} = \frac{\langle\Psi|H|\Psi\rangle}{\langle\Psi|\Psi\rangle}. \tag{10}$$

In this way the correlation energy, $E_{\rm corr} = E_{\rm tot} - E_{\rm HF}$, was obtained. The correlation operators

$$O_m \equiv \delta n_{i\mu\sigma}\delta n_{i\nu\sigma}, \tag{11}$$

where $\delta n_{i\mu\sigma}$ are density fluctuations, include the set of all possible $\delta n_{i\mu\sigma}\delta n_{i\nu\sigma'}$ on-site operators (defined separately for each site i). The symbol δ in $\delta n_{i\mu\sigma}$ indicates taking *only that part* of $n_{i\mu\sigma}$ operator which annihilates one electron in an occupied single particle state from the HF ground state $|\Phi_0\rangle$, and creates an electron in one of the virtual states. The above local operators O_m defined in equation (11) (in the present model) correspond to the subselection of the most important two electron excitations within the *ab initio* configuration-interaction method. For more technical details see [10, 44].

Let us note that three, four, or more electron excitations are also important (in the intermediate and strong correlation regime). However, as yet there is no controlled and/or efficient method of implementing them for large systems (what we mean here is for example a variant of the multiconfiguration self-consistent field method augmented with averaged coupled cluster approach working for clusters containing more than a dozen of sites). Therefore, such excitations were neglected.

For a given doping x we performed the HF computations starting from a given configuration of initial conditions, i.e., from predefined charge and spin configuration, predefined pattern of core t_{2g} spins (taken as frozen), and a predefined set of classical $\{Q_{2i}, Q_{3i}\}$ variables. The predefined core spin patterns we took into account are shown in figure 1. For each individual fixed set of initial conditions we obtain on convergence the HF energy $E_{\rm HF}$ and the HF wavefunction $|\Phi_0\rangle$ accompanied by the optimized set of JT deformations—$\{Q_{2i}\}$ and $\{Q_{3i}\}$. Then, after finishing self-consistent HF runs (still for the same set of fixed initial conditions) we performed correlation computations and obtained the total energy $E^{(1)}_{\rm tot}$ (10).

Next the same procedure was applied to a second set of fixed HF initial conditions to determine the corresponding local energy minimum $E^{(2)}_{\rm tot}$ for this configuration. In this way we treated the entire set of HF initial conditions used in the present calculations. Finally, the resulting set of total energies $\{E^{(n)}_{\rm tot}\}$ for different locally stable states $\{|\Psi^{(n)}\rangle\}$ was inspected and the lowest energy state was identified as a good candidate for the true ground state (for given Hamiltonian parameters; we remind the reader that this is in all cases the ground state at zero temperature).

3. Results

In general the computations are costly and time consuming, if one wants to obtain unbiased results. We used more than thousand different initial conditions for each set of Hamiltonian parameters, and as we have found, *a posteriori*, any smaller number would certainly not suffice to cover all *a priori* possible states. This large number corresponds to the many potential possibilities of symmetry breaking in the bilayer system.

First, the considered states belong to two classes: (i) either the e_g electrons in the ground state are all polarized in the FM state, e.g. all spins pointing upwards, or (ii) the number of up and down electrons is equal in the AF configuration (zero total magnetization). For each one of these possibilities we need separate HF and correlation calculations. All these potentially possible configurations are in fact induced by the orientation of core t_{2g} spins (here assumed fixed and frozen). For each doping we examined only the 8 possibilities of magnetically ordered phases which are sketched in figure 1, in particular five phases: G-type antiferromagnet, so-called G-AF phase; zig-zag CE-type AF phase [45]; C-AF configuration (vertical FM order with AF coupling between the alternating lines of up and down spins), and A-AF phase with FM planes coupled by AF interactions. The other 3 phases shown in figure 1, A′-AF, C′-AF and CE′ phase, correspond to the reversed sign of the inter-layer coupling, i.e., between upper and lower planes of the bilayer. We believe that the present set captures the essential states realized experimentally [18], and other spin configurations were not taken into account (though certainly examination of some random arrangements of core spins could be of interest, in particular for large doping of $x \sim 0.7$ where a glassy phase was reported).

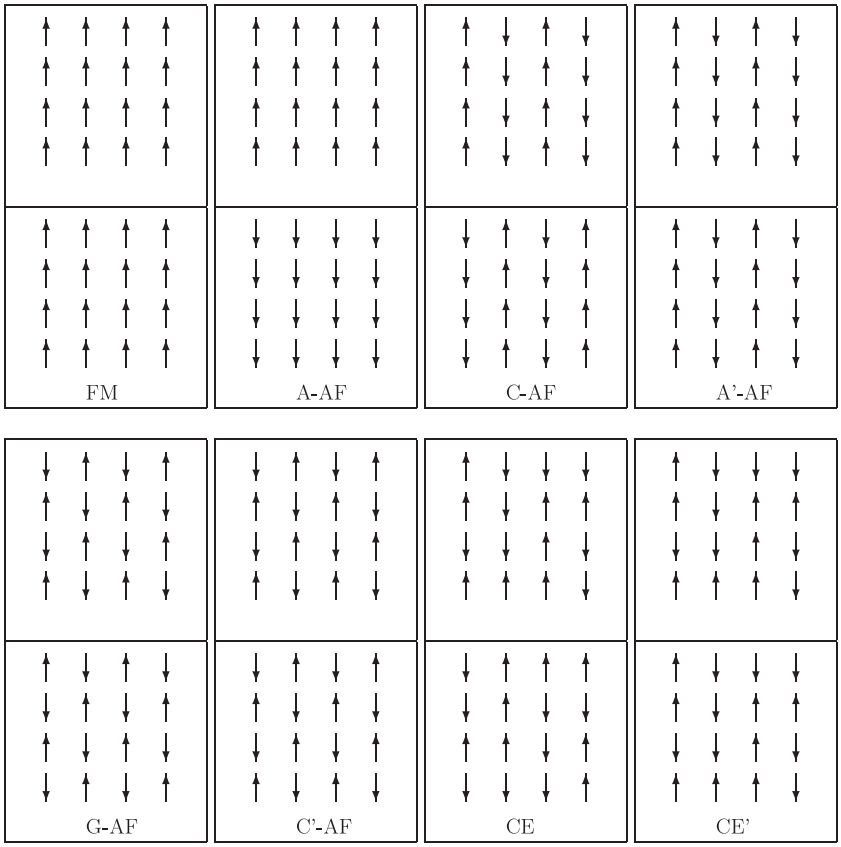

Figure 1. The possible types of magnetic order of t_{2g} core spins in $4 \times 4 \times 2$ cluster. The upper/lower panel for each phase corresponds to the upper/lower plane of the bilayer, respectively. The acronyms we use for the description of the individual magnetic phases are simplified (for the needs of the present model) variants of acronyms used in the literature [9, 10, 18]. Concerning the spin zig-zag CE phase, note that zig-zag lines of up (down) spins are fully visible only when the periodic boundary conditions of the 4×4 clusters in each layer are taken into account.

After fixing a core spin configuration, various starting configurations of e_g spins and charges (random arrangements) were tried and the system was iterated until convergence. For $\{Q_{2i}\}$ and $\{Q_{3i}\}$ variables we used zero (uniform) starting values, and the system adjusted to proper finite values through the iterations. As expected, the final directions of e_g spins in the converged states (on-sites with non-negligible e_g charge) were found to be parallel to those of the core t_{2g} spins as long as J_H was finite (this was checked during each computer run). This confirms that Hund's exchange plays a prominent role in local moment formation, as found before both in transition metals [46] and in doped correlated insulators [9, 47].

Virtually, each set of initial conditions leads to some *a priori* metastable state. Most of them are separated by a tiny energy interval (typically only of the order of 0.01 eV for the entire cluster). Thus identification of the true ground state turns out to be somewhat problematic. To become reasonably certain one must examine few hundred of such metastable states. Even when such a large sample is available one cannot exclude the possibility that another configuration might be more stable in some cases. Namely, the change of any of the employed approximations and assumptions can (in principle) reverse the order of the ground state with one of the neighbouring 'metastable' states. Take, for example, the assumption that the core spins are frozen. One can easily imagine that unfreezing them, i.e. allowing for quantum fluctuations in AF local configurations, could lower the ground state energy more in one spin configuration than in another one by the order of 0.01 eV, which would be just sufficient to trigger the discussed crossover between two phases. The same holds true for: (i) somewhat better treatment of electron correlations, (ii) including weak nearest neighbour inter-site Coulomb repulsion, (iii) including next-nearest-neighbour hopping, and finally (iv) considering more elaborate JT couplings which involves three sites (e.g. as introduced in [30]).

Unfortunately, the entire phase diagram of the bilayer system (when changing all Hamiltonian parameters and doping) is numerically too expensive. Thus in this paper only several isolated (but well motivated) points in the parameter space were inspected in detail. The obtained stable configurations for selected doping in the range $0.31 < x < 0.88$ and for different values of Hund's exchange J_H are presented in table 1. The selected doping levels correspond (approximately) to the following numbers of holes $n_h = 10, 12, 14, \ldots, 28$, doped in half-filled configuration of the considered $4 \times 4 \times 2$ cluster. We notice that the central column, i.e. the one corresponding to $J_H = 0.7$ eV, reproduces the experimental data [18] reasonably well. There are two differences: (i) for the doping $x = 0.69$ we obtained C-AF, while the experiment data point out towards some unspecified

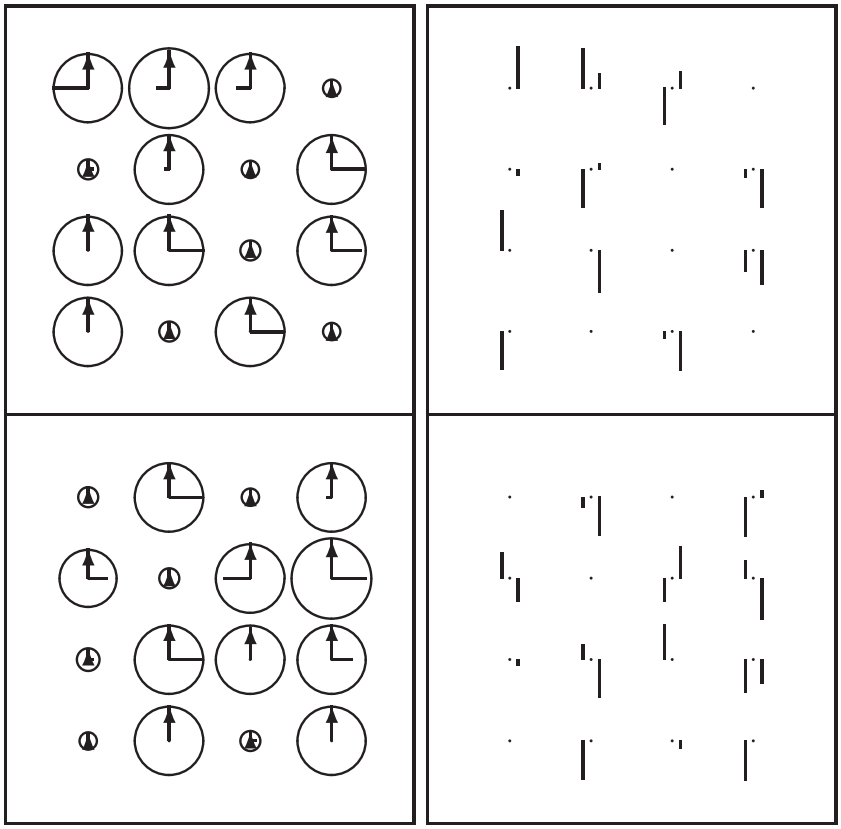

Figure 2. The FM ground state with nonuniform charge distribution obtained for doping $x = 0.38$. The orbital occupancy is also nonuniform with a slightly higher electron density in the $x^2 - y^2$ orbital than in the $3z^2 - r^2$ one. Left upper and left lower panels: magnetic, charge and orbital order for e_g electrons as obtained in the $4 \times 4 \times 2$ cluster (upper and lower planes of the bilayer) with 12 doped holes at half-filling ($x = 0.38$). Core t_{2g} spins are not shown. Right upper and right lower panels: the corresponding JT distortions (upper and lower planes of the bilayer). Parameters of the Hamiltonian: $t_0 = 0.4$ eV, $U = 8t_0$ eV, $J_H = 0.7$ eV, $K = 13$ eV Å^{-2}, $g = 3.8$ eV Å^{-1}, $J' = 4.0$ meV and $E_z = 0$ eV. The ground state energies are: $E_{HF} = -36.264$ eV, $E_{tot} = -36.277$ eV.

Table 1. Magnetic order as obtained in the ground state of a $4 \times 4 \times 2$ cluster for selected values of Hund's exchange interaction J_H (in eV) and for increasing doping x. Other parameters of the Hamiltonian (1): $t_0 = 0.4$ eV, $U = 8t_0$, $K = 13$ eV Å^{-2}, $g = 3.8$ eV Å^{-1}, $J' = 4.0$ meV and $E_z = 0$.

J_H (eV) → x ↓	0.9	0.8	0.7	0.6	0.5	0.0
0.31	FM	FM	FM	FM	CE′	G-AF
0.38	FM	FM	FM	FM	CE	G-AF
0.44	FM	A-AF	A-AF	CE	CE	G-AF
0.50	CE	A-AF	CE	CE	CE	G-AF
0.56	FM	FM	A-AF	A-AF	CE	G-AF
0.62	A-AF	A-AF	A-AF	A-AF	A-AF	G-AF
0.69	A-AF	A-AF	C-AF	C-AF	C-AF	G-AF
0.75	C-AF	C-AF	C-AF	C-AF	C-AF	G-AF
0.81	A′-AF	C-AF	C-AF	C-AF	C-AF	G-AF
0.88	A′-AF	A′-AF	A′-AF	A′-AF	A′-AF	G-AF

Table 2. Magnetic order as obtained in the ground state of a $4 \times 4 \times 2$ cluster with two values of $U = 6t_0$ and $10t_0$, a few selected values of Hund's exchange interaction J_H (in eV), and for increasing doping x. Other parameters of the Hamiltonian (1) as in table 1.

	$U = 6t_0$			$U = 10t_0$		
J_H (eV) → x ↓	0.9	0.7	0.5	0.9	0.8	0.7
0.31	FM	FM	FM	FM	FM	FM
0.38	FM	FM	CE’	FM	FM	A-AF
0.44	FM	FM	CE	A-AF	A-AF	A-AF
0.50	FM	CE	CE	A-AF	A-AF	CE
0.56	A-AF	A-AF	A-AF	A-AF	A-AF	A-AF
0.62	FM	A-AF	A-AF	A-AF	A-AF	A-AF
0.69	FM	A-AF	C-AF	A-AF	C-AF	C-AF
0.75	C-AF	C-AF	C-AF	C-AF	C-AF	C-AF
0.81	A′-AF	C-AF	C-AF	C-AF	C-AF	C-AF
0.88	A′-AF	A′-AF	A′-AF	A′-AF	A′-AF	A′-AF

magnetic glassy phase; (ii) for the doping $x = 0.88$ we get A′-AF instead of C-AF (our inter-layer coupling is FM instead of the AF one suggested by the experimental results; still the most stable order for a single plane is of the C-type as expected). These results are robust as the analogous column for $J_H = 0.65$ eV (not shown in table 1) is the exact copy of the column corresponding to $J_H = 0.7$ eV. Altogether, by making a comparison of table 1 with table 2 and with other similar results (obtained for different parameters, not shown) we could conclude that the most realistic parameter set which is able to reproduce the essential features of the bilayer manganites consists of the following parameters of the

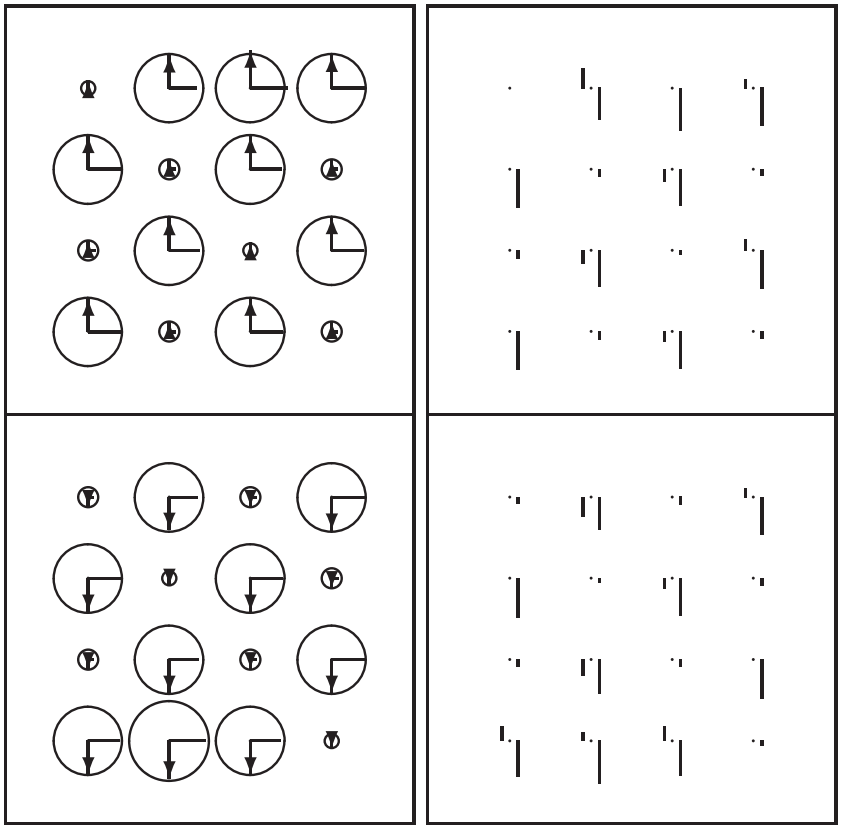

Figure 3. The A-AF ground state with nonuniform charge distribution for the doping of $x = 0.44$ (14 doped holes in the half-filled $4 \times 4 \times 2$ cluster). The orbital ordering is uniform—mostly $x^2 - y^2$ orbitals are occupied. The legend and the parameters of the Hamiltonian are the same as in figure 2. The ground state energies are: $E_{\rm HF} = -33.383$ eV, $E_{\rm tot} = -33.394$ eV.

Table 3. Magnetic order as obtained in the ground state of a $4 \times 4 \times 2$ cluster for selected values of the crystal field E_z (in eV) and increasing doping x. Other parameters of the Hamiltonian (1): $t_0 = 0.4$ eV, $U = 8t_0$, $J_{\rm H} = 0.7$ eV, $K = 13$ eV Å^{-2}, $g = 3.8$ eV Å^{-1}, $J' = 4.0$ meV.

E_z (eV) → x ↓	−0.2	+0.2	−0.1	+0.1
0.31	CE′	A-AF	CE′	A-AF
0.38	A′-AF	A-AF	FM	A-AF
0.44	A′-AF	A-AF	A′-AF	A-AF
0.50	C′-AF	A-AF	A′-AF	A-AF
0.56	C′-AF	A-AF	A′-AF	A-AF
0.62	A′-AF	A-AF	A′-AF	A-AF
0.69	A′-AF	A-AF	A′-AF	A-AF
0.75	C-AF	C-AF	C-AF	C-AF
0.81	A′-AF	C-AF	A′-AF	C-AF
0.88	A′-AF	C-AF	A′-AF	C-AF

effective Hamiltonian (1): $t_0 = 0.4$ eV, $U = 8t_0$, $K = 13$ eV Å^{-2}, $g = 3.8$ eV Å^{-1}, $J' = 4.0$ meV and $E_z = 0$ and $J_{\rm H} = 0.65$–0.7 eV.

Finally, as the last set we present the data of table 3 which support our belief that the crystal field in the bilayer $La_{2-2x}Sr_{1+2x}Mn_2O_7$ manganite is very small and may be well approximated by $E_z = 0$ (contrary to the orbital splitting in monolayer manganites [10]). Indeed, the sequence of the ground states obtained for $E_z \neq 0$ versus doping does not reproduce the experimental data (which is best visible for the case of lower dopings).

Altogether, by looking at the data in tables 1–3, we could identify certain simple and persistent generic trends in the multidimensional phase diagram which correspond to the experimental observations. It is important that $\{|x\rangle, |z\rangle\}$ orbitals are almost degenerate ($E_z \simeq 0$) as only then is the FM order with disordered orbitals in the orbital liquid state [16] stable, in agreement with experiment. At doping $x > 0.5$ various AF phases are stable. The generic type of order in this regime is the A-AF phase, with the AF coupling between the FM planes of the bilayer. However, when the doping is high $x \simeq 0.75$ and Hund's exchange is not too strong $J_{\rm H} \simeq 0.7$, the FM bonds in the planes weaken and another instability towards the C-AF phase occurs, in agreement with experiment [18] and with other model calculations [9, 26]. This latter result is robust and is remains unchanged when the value of U is varied in the expected regime of $6t_0 < U < 10t_0$. In fact, the e_g electrons are already strongly correlated at $U = 6t_0$, so the magnetic order depends only on the other parameters.

The data contained in tables 1–3 analyzed above focus on the variation of the magnetic order in the ground state with increasing doping x. One has to supplement the results for the magnetic order with information about the charge order and the orbital order and their variation with doping. We present the respective data in figures 2–5. Therein we have chosen the following conventions: at each site the circle radius

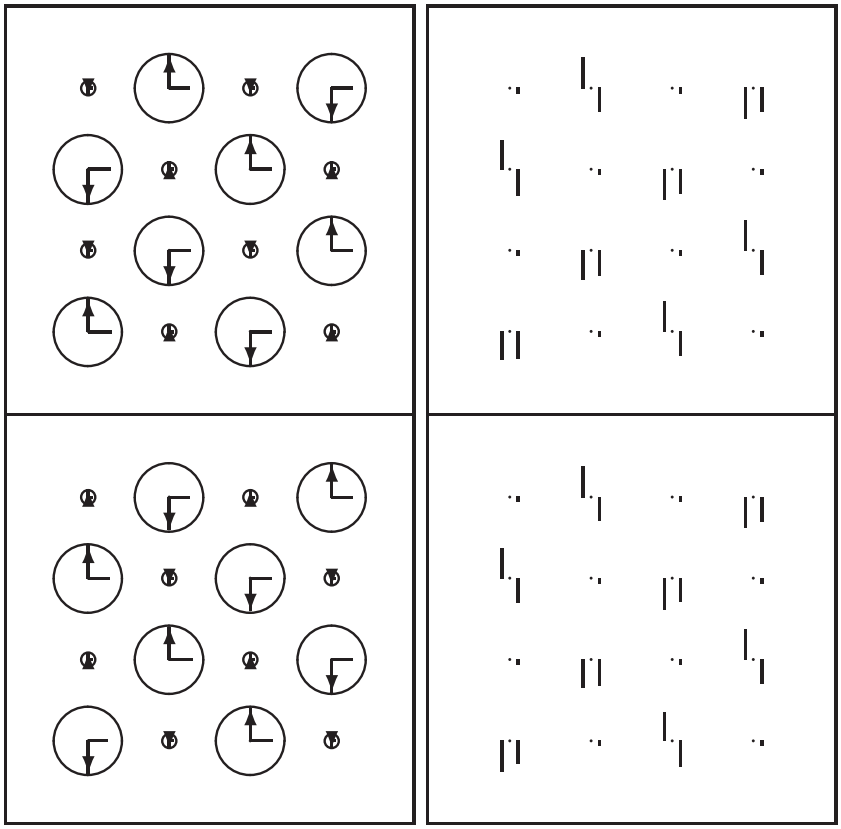

Figure 4. The CE phase with (checker-board) charge order in the ground state obtained for $x = 0.5$ doping (16 doped holes in the half-filled $4 \times 4 \times 2$ cluster). The orbital polarization is uniform—mostly $x^2 - y^2$ orbitals are occupied. The legend and the parameters of the Hamiltonian are the same as in figure 2. The ground state energies are: $E_{\rm HF} = -30.311$ eV, $E_{\rm tot} = -30.351$ eV. For the converged A-AF metastable ground state we obtained the ground state energies $E_{\rm HF} = -30.339$ eV, $E_{\rm tot} = -30.349$ eV.

corresponds to the e_g on-site total charge multiplied by 0.5; the arrow length to the total e_g spin; the horizontal bar length (upper left and lower left panels of the bilayer) to the charge density difference between $x^2 - y^2$ and $3z^2 - r^2$ orbitals (namely—a bar-to-the-right with value of 0.5 corresponds to pure $x^2 - y^2$ occupation, a bar-to-the-left with value of -0.5 corresponds to pure $3z^2 - r^2$ occupation, a dot, i.e. the absence of the bar, corresponds to identical charge densities in both orbitals (the amplitude of mixing was not computed in the program)). On the right panels at each site (site shown as a dot) two vertical bars are shown, the one slightly to the left (from the dot) denotes twice the Q_{2i} JT distortion and the one slightly to the right denotes twice the Q_{3i} one (bars directed upwards are for positive, and the bars directed downwards for negative values). All these values are expressed proportionally to the nearest neighbour site–site distance which is assumed to be unity. Note that the pictures shown in the panels of figures 2–5 were generated automatically by the program as separate output files in LaTex. Thus the radii of the circles are only approximately proportional to the actual charge densities (being closest to the circles predefined in the LaTex graphical package).

The evolution of charge distribution found for the realistic parameter set is rather simple to describe. At small dopings the FM order is present (for $0.3 < x < 0.4$), and it is accompanied by the nonuniform charge distribution. This results from local JT distortions around the Mn^{3+} ions occupied by an e_g electron. Therefore, one could call the states obtained at doping $x = 0.38$ local polarons (see figure 2). We believe that these states are responsible for the insulating nature of the paramagnetic state above the magnetic transition, observed in the FM bilayer manganites [48]. As the doping x increases and approaches the value $x = 0.5$ this charge modulation is quickly amplified (see figure 3), and at the precise value of $x = 0.5$ one obtains perfect charge order of the simple checker-board type accompanied by the CE magnetic order shown in figure 4.

Consider now the orbital states for increasing doping x. For FM order ($x \simeq 0.3$) we obtained that electrons are distributed over $x^2 - y^2$ and $3z^2 - r^2$ orbitals (see right- and left-directed horizontal bars in figure 2; when the bars reduce to the dots one finds almost equal electron densities in either orbital state). This situation corresponds to the orbital liquid disordered state [16] and results in rather strong double exchange FM interactions [33]. They occur here in a bilayer system in spite of its reduced symmetry as compared with the reference $La_{1-x}Sr_xMnO_3$ perovskites. When x increases then the orbitals soon become polarized and electrons predominantly occupy the $x^2 - y^2$ states, similar to a single layer in $La_{2-x}Sr_xMnO_4$ [49]—the admixture of $3z^2 - r^2$ character, which results from the nonconservation of the orbital flavour with the hopping process, is finite but remains rather small. This change in the orbital occupancy

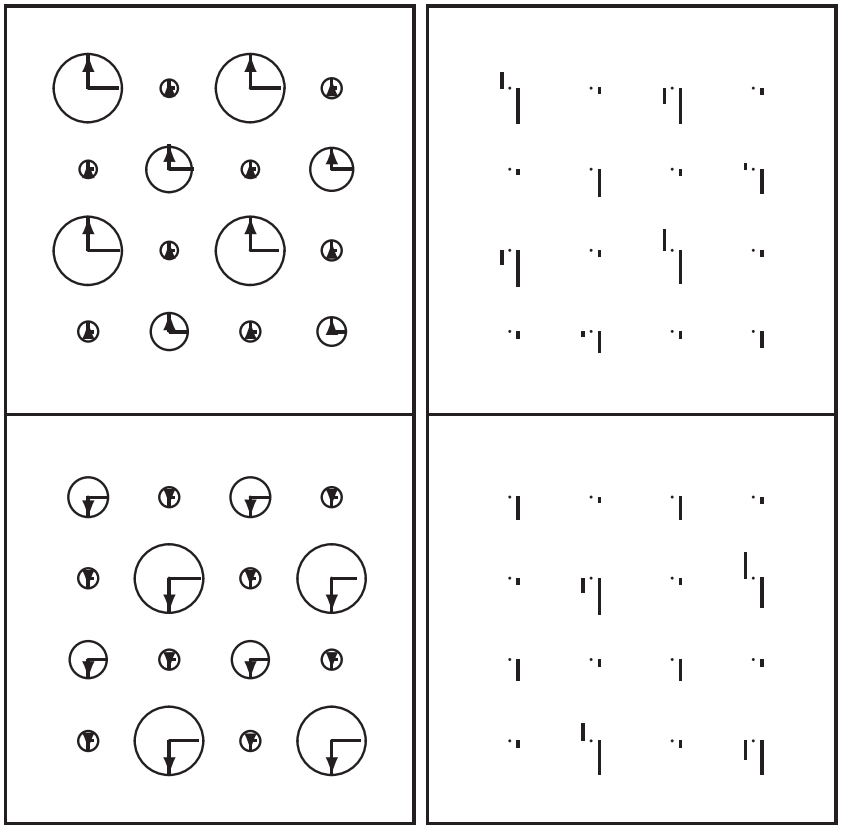

Figure 5. The A-AF phase with nonuniform charge distribution in the ground state obtained for the doping of $x = 0.56$ (18 doped holes in the half-filled $4 \times 4 \times 2$ cluster). The orbital ordering is uniform—predominantly $x^2 - y^2$ orbitals are occupied. The legend and the parameters of the Hamiltonian are the same as in figure 2. The ground state energies are: $E_{\rm HF} = -26.820$ eV, $E_{\rm tot} = -26.835$ eV.

gradually destabilizes the FM phase [33], and the magnetic order changes to the A-AF one at $x \simeq 0.45$. These findings are in very good agreement with the experimental data [17–22, 24].

The case of $x = 0.5$ doping is of particular interest. Experimentally the CE phase was difficult to detect and was only reported in bilayer manganites quite recently [24]. According to our model calculations, the A-AF phase would be stable if neglecting electronic correlations, but when the correlation effects are included the CE phase (see figure 4) takes over. In fact, the difference between the energies of the A-AF and CE phase (see the caption of figure 4) is so small in the framework of the present model that one might assume that both of them are good candidates for the true ground state. The CE order is known to be quite fragile in the purely electronic models and is destabilized by increasing U when the HF approximation is used [50]. We therefore emphasize that local electronic correlations play a very important role and stabilize this phase for $x = 0.5$ doping in the range of realistic values $J_{\rm H} \simeq 0.7$ eV (see tables 1 and 2), in agreement with recent experimental data [24].

For further increased doping $x > 0.5$ the spatial charge modulation gradually disappears (see figure 5) and for larger values of x we get a uniform charge distribution with $x^2 - y^2$ orbitals occupied and only negligible occupancy of $3z^2 - r^2$ orbitals (not shown). This latter result is expected as more kinetic energy is gained when orbitals are polarized in $x^2 - y^2$ states in layered systems [49]. Under these circumstances the A-AF phase is favoured. A certain reorganization of orbital occupancies, with somewhat increased density in $3z^2 - r^2$ orbitals, accompanies an instability towards the C-AF phase which occurs in a range of doping around $x = 0.75$ (see tables 1 and 2).

Our results reveal the generic presence of finite JT distortions at least on charge-majority sites. In general Q_3 are negative while Q_2 in turn takes on positive and negative values in such a way that the lattice is distorted locally, as shown schematically in [28] but the global (unidirectional) distortion of the lattice is absent (best seen in figure 4). To obtain a better overall insight into the gradual changes of charge distribution with increased doping (particularly there where some large changes occur) look at figures 2–5.

To finish the discussion of the results we would like to point out that the obtained amplitudes of charge modulation (between charge-majority and charge-minority sites) is in our opinion larger than that obtained in the experiment [40]. This is (i) an artefact of the effective model given in equation (1) on the one hand, and (ii) due to finite size effects on the other. First of all, let us note that the definition of local charge centred at a given Mn ion is not unique. While the experiment gives information about true atomic charges, the d states in the present effective model represent not just individual Mn ions but rather Wannier orbitals centred on them. It is to be expected that each Wannier orbital extends not only up to neighbouring oxygens but up to further Mn ions (so-called orthogonalization

tails). In other words, in the present effective model (1) charge differences between Wannier orbitals at different sites can be large. However, when this is translated to the real space corresponding to real crystal structure, then the charges on Mn ions would be smeared out due to overlap (with other Wannier orbitals) and the charge modulation between individual Mn ions would be considerably reduced. Secondly, only discrete energy spectra are realized in the present cluster calculations, while the distribution of eigenstates is continuous in a metal and the metallic screening is expected to reduce the amplitude of charge modulation.

4. Summary

We have analyzed an effective theoretical model (1) for bilayer manganites. It includes all essential features of strongly correlated electrons in partly filled e_g orbitals, such as: (i) their anisotropic phase dependent hopping, (ii) large on-site electron interactions described by the Coulomb U, and (iii) the coupling of e_g electron spins to frozen spins of core t_{2g} electrons at Mn ions by Hund's exchange J_H. The joint effect of large Coulomb interactions and of the JT interactions with the lattice plays a crucial role in the observed types of magnetic order in the bilayer manganites [18], so we conclude that the observed phase diagram follows from the competition between different trends and intrinsic frustration of microscopic interactions, similar to the one known for the doped perovskite manganites.

Our effective model reproduced the experimental phase diagram for the doped bilayer $La_{2-2x}Sr_{1+2x}Mn_2O_7$ manganites. We have shown that calculations beyond the commonly employed Hartree–Fock approximation are necessary and local electronic correlations play a very important role in obtaining qualitatively correct phase diagram. *Inter alia*, these correlations are responsible for the subtle stability of the CE phase in the half-doped bilayer manganites. This demonstrates that the CE-type of order is very subtle, and lattice effects such as next-nearest-neighbour JT interactions might be necessary to stabilize it not only in monolayer [30], but also in bilayer manganites.

Altogether, we conclude that the effective model (1) performs reasonably well and is able to reproduce qualitatively all the systematic changes in magnetic, orbital and charge order observed in the bilayer manganites. Therefore, we expect that the present model provides a good starting point to investigate the stability of magnetic phases in other complex systems, such as perovskite manganites and manganite interfaces.

Acknowledgments

This work was supported by the Polish Ministry of Science and Higher Education under Project No. N202 068 32/1481. A M Oleś acknowledges support by the Foundation for Polish Science (FNP).

References

[1] Dagotto E, Hotta T and Moreo A 2001 *Phys. Rep.* **344** 1
Dagotto E 2005 *New J. Phys.* **7** 67
[2] Weisse A and Fehske H 2004 *New J. Phys.* **6** 158
[3] Hotta T, Malvezzi A L and Dagotto E 2000 *Phys. Rev.* B **62** 9432
[4] Millis A J 1996 *Phys. Rev.* B **53** 8434
Millis A J 1997 *Phys. Rev.* B **55** 6405
[5] Feiner L F and Oleś A M 1999 *Phys. Rev.* B **59** 3295
[6] Oleś A M, Khaliullin G, Horsch P and Feiner L F 2005 *Phys. Rev.* B **72** 214431
[7] Mizokawa T and Fujimori A 1997 *Phys. Rev.* B **56** R493
[8] Dagotto E, Yunoki S, Malvezzi A L, Moreo A, Hu J, Capponi S, Poilblanc D and Furukawa N 1998 *Phys. Rev.* B **58** 6414
[9] Daghofer M, Oleś A M, Neuber D and von der Linden W 2006 *Phys. Rev.* B **73** 104451
Daghofer M, Oleś A M and von der Linden W 2004 *Phys. Rev.* B **70** 184430
Daghofer M, Oleś A M and von der Linden W 2005 *Phys. Status Solidi* b **242** 311
Daghofer M and Oleś A M 2007 *Acta Phys. Pol.* A **111** 497
[10] Rościszewski K and Oleś A M 2007 *J. Phys.: Condens. Matter* **19** 186223
Rościszewski K and Oleś A M 2005 *Phys. Status Solidi* b **243** 155
[11] Jung J H, Ahn J S, Yu J, Noth T W, Lee J, Moritomo Y, Solovyev I and Terakura K 2000 *Phys. Rev.* B **61** 6902
[12] Park K T 2001 *J. Phys.: Condens. Matter* **13** 9231
[13] Yin W-G, Volja D and Ku W 2006 *Phys. Rev. Lett.* **96** 116405
[14] Yamasaki A, Feldbacher M, Yang Y-F, Andersen O K and Held K 2006 *Phys. Rev. Lett.* **96** 166401
[15] Oleś A M and Feiner L F 2002 *Phys. Rev.* B **65** 052414
[16] Feiner L F and Oleś A M 2005 *Phys. Rev.* B **71** 144422
[17] Kubota M, Yoshizawa H, Morimoto Y, Fujioka H, Hirota K and Endoh Y 1999 *J. Phys. Soc. Japan* **68** 2202
Kubota M, Fujioka H, Hirota K, Ohoyama K, Morimoto Y, Yoshizawa H and Endoh Y 2000 *J. Phys. Soc. Japan* **69** 1606
[18] Ling C D, Millburn J E, Mitchell J F, Argyriou D N, Linton J and Bordallo H N 2000 *Phys. Rev.* B **62** 15096
[19] Perring T G, Adroja D T, Caboussant G, Aeppli G, Kimura T and Tokura Y 2001 *Phys. Rev. Lett.* **87** 217201
[20] Wilkins S B, Spencer P D, Beale T A, Hatton P D, v Zimmermann M, Brown S D, Prabhakaran D and Boothroyd A T 2003 *Phys. Rev.* B **67** 205110
Wilkins S B, Stojic N, Beale T A, Binggeli N, Hatton P D, Bencok P, Stanescu S, Mitchell J F, Abbamonte P and Altarelli M 2006 *J. Phys.: Condens. Matter* **18** L323
[21] Qiu X, Billinge S L, Kmety C R and Mitchell J F 2004 *J. Phys. Chem. Solids* **65** 1423
[22] Wang A, Liu T, Liu Y and Cao G 2005 *Physica* B **363** 115
[23] Beale T A, Spencer P D, Hutton P D, Wilkins S B, v Zimmermann M, Brown S D, Prabhakaran D and Boothroyd A T 2005 *Phys. Rev.* B **72** 064432
[24] Li Q A, Gray K E, Zheng H, Claus H, Rosenkrantz S, Nyborg Ancona S, Osborn R, Mitchell J F, Chen Y and Lynn J W 2007 *Phys. Rev. Lett.* **98** 167201
[25] Popovic Z and Satpathy S 2000 *Phys. Rev. Lett.* **84** 1603
[26] Maitra T and Taraphder A 2004 *Europhys. Lett.* **65** 262
Maitra T, Taraphder A and Beck H 2005 *J. Phys.: Condens. Matter* **17** 4333
[27] Salafranca J and Brey L 2006 *Phys. Rev.* B **73** 024422
[28] Zaanen J and Oleś A M 1993 *Phys. Rev.* B **48** 7197
[29] Oleś A M 1983 *Phys. Rev.* B **28** 327
[30] Bała J, Horsch P and Mack F 2004 *Phys. Rev.* B **69** 094415
Bała J and Horsch P 2005 *Phys. Rev.* B **72** 012404
[31] Bocquet A E, Mizokawa T, Saitoh T, Namatame H and Fujimori A 1992 *Phys. Rev.* B **46** 3771
Chainani A, Mathew M and Sarma D 1993 *Phys. Rev.* B **47** 15397
Arima T, Tokura Y and Torrance J B 1993 *Phys. Rev.* B **48** 17006
Saitoh T, Bocquet A E, Mizokawa T, Namatame H, Fujimori A, Abbate A, Takeda Y and Takano M 1995 *Phys. Rev.* B **51** 13942

[32] Shannon N, Chatterji T, Ouchni F and Thalmeier P 2002 *Eur. Phys. J.* B **27** 287
[33] Oleś A M and Feiner L F 2003 *Phys. Rev.* B **67** 092407
[34] Kovaleva N N, Boris A V, Bernhard C, Kilakov A, Pimenov A, Balbashov A M, Khaliullin G and Keimer B 2004 *Phys. Rev. Lett.* **93** 147204
[35] Okimoto Y, Kasufuji T, Ishikawa T, Urushibara A, Arima T and Tokura Y 1995 *Phys. Rev. Lett.* **75** 109
[36] Feinberg D, Germain P, Grilli M and Seibold G 1998 *Phys. Rev.* B **57** R5583
[37] Kawano H, Kojimoto R, Kubota M and Yoshizawa H 1996 *Phys. Rev.* B **53** R14709
[38] Bala J and Oleś A M 2000 *Phys. Rev.* B **62** R6085
Bala J, Oleś A M and Sawatzky G A 2002 *Phys. Rev.* B **65** 184414
[39] Tyer R, Temmerson W M, Szostek Z, Banach G, Svane A and Gehring G A 2004 *Europhys. Lett.* **65** 519
[40] Larochelle S, Mehta A, Lu L, Mang P K, Vajk O P, Kaneko N, Lynn J W, Zhou L and Greven M 2005 *Phys. Rev.* B **71** 024435
[41] Jackeli G and Perkins N B 2002 *Phys. Rev.* B **65** 212402
[42] Moritomo Y, Arima T and Tokura Y 1995 *J. Phys. Soc. Japan* **64** 4117
[43] Stollhoff G and Fulde P 1980 *J. Chem. Phys.* **73** 4548
Stollhoff G 1996 *J. Chem. Phys.* **105** 227
Fulde P 1991 *Electron Correlations in Molecules and Solids* (*Springer Series in Solid State Sciences* vol 100) (Berlin: Springer)
[44] Góra D, Rościszewski K and Oleś A M 1999 *Phys. Rev.* B **60** 7429
Rościszewski K and Oleś A M 2003 *J. Phys.: Condens. Matter* **15** 8363
[45] Sternlieb B J, Hill J P, Wildgruber U C, Luke G M, Nachumi B, Morimoto Y and Tokura Y 1996 *Phys. Rev. Lett.* **76** 2169
Park J H, Chen C T, Cheong S, Bao W, Meigs G, Chakarian V and Izeda Y U 1996 *Phys. Rev. Lett.* **76** 4215
Chatterji T, Fauth F, Ouladdiaf B, Mandal P and Ghosh B 2003 *Phys. Rev.* B **68** 052406
Huang D J, Wu W B, Guo G Y, Lin H J, Hou T Y, Chang C F, Chen C T, Fujimori A, Kimura T, Huang H B, Tanaka A and Jo T 2004 *Phys. Rev. Lett.* **92** 087202
[46] Oleś A M and Stollhoff G 1984 *Phys. Rev.* B **29** 314
Stollhoff G, Oleś A M and Heine V 1990 *Phys. Rev.* B **41** 7028
Fleck M, Oleś A M and Hedin L 1997 *Phys. Rev.* B **56** 3159
[47] Raczkowski M, Frésard R and Oleś A M 2006 *Phys. Rev.* B **73** 094429
Frésard R, Raczkowski M and Oleś A M 2005 *Phys. Status Solidi* b **242** 370
[48] Moussa F, Hennion M, Wang F, Gukasov A, Suryanarayanan R, Apostu M and Revcolevschi A 2004 *Phys. Rev. Lett.* **93** 107202
[49] Mack F and Horsch P 1999 *Phys. Rev. Lett.* **82** 3160
[50] van den Brink J, Khaliullin G and Khomskii D 1999 *Phys. Rev. Lett.* **83** 5118